Supporting Information

Synthesis and Characterization of 3,5-Bis(di-*tert*-butylphosphinito)pyridine Pincer Complexes

Nicholas A. Swisher and Robert H. Grubbs

Arnold and Mabel Beckman Laboratories of Chemical Synthesis, California Institute of Technology, Pasadena, California 91125, United States

Table of Contents:

Nuclear Magnetic Resonance Spectra
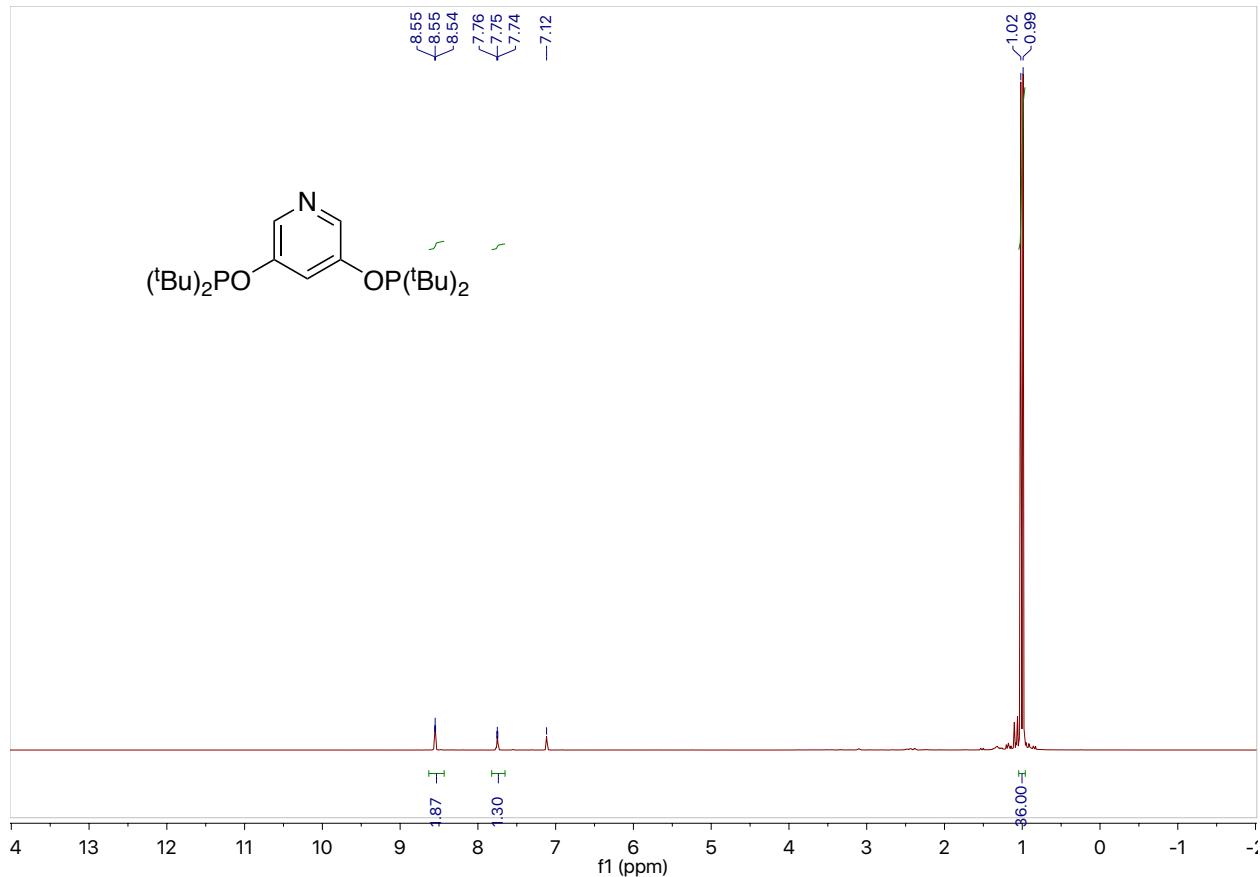
Figure S1. ¹H NMR (400 MHz, C₆D₆) spectrum of 3,5-bis(di-*tert*-butylphosphinito)pyridine, **1**.
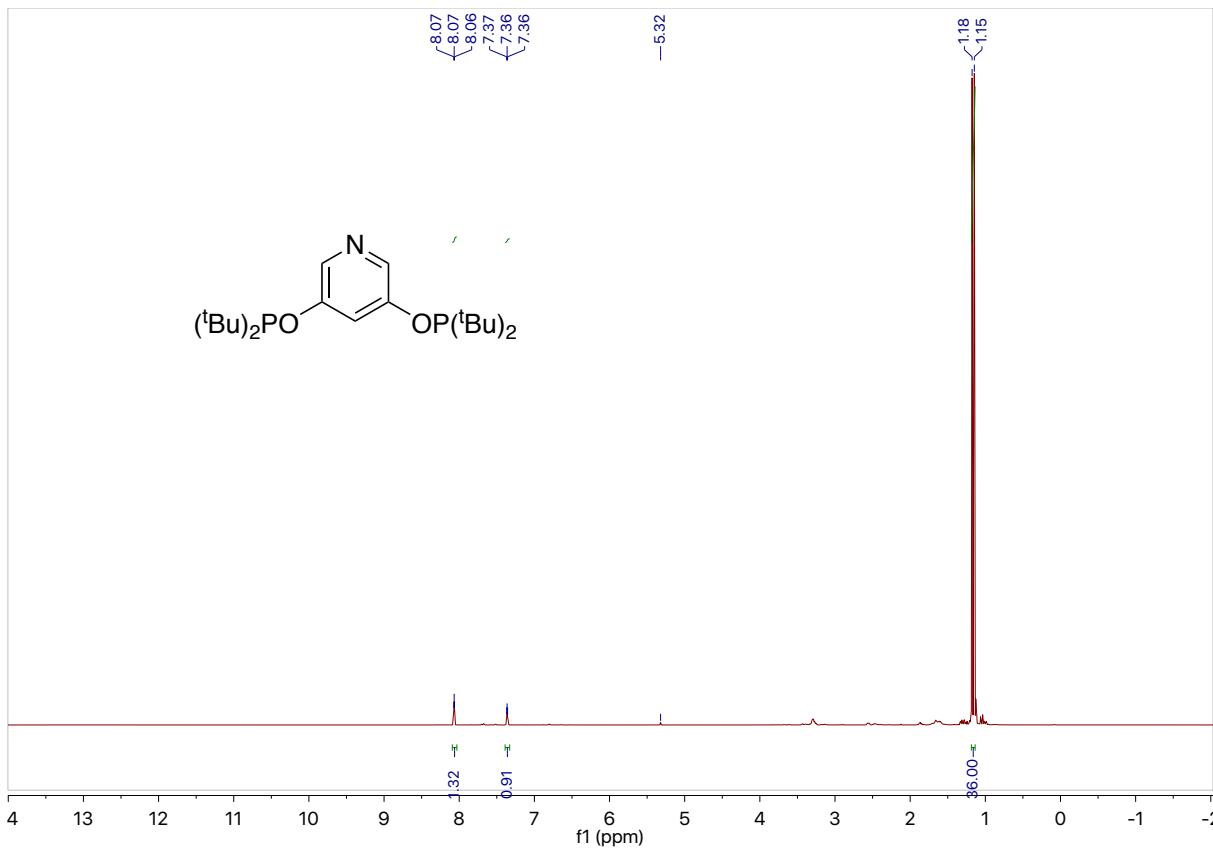
**Figure S2**. ^{1}H NMR (400 MHz, CD$_2$Cl$_2$) spectrum of 3,5-bis(di-*tert*-butylphosphinito)pyridine, **1**.
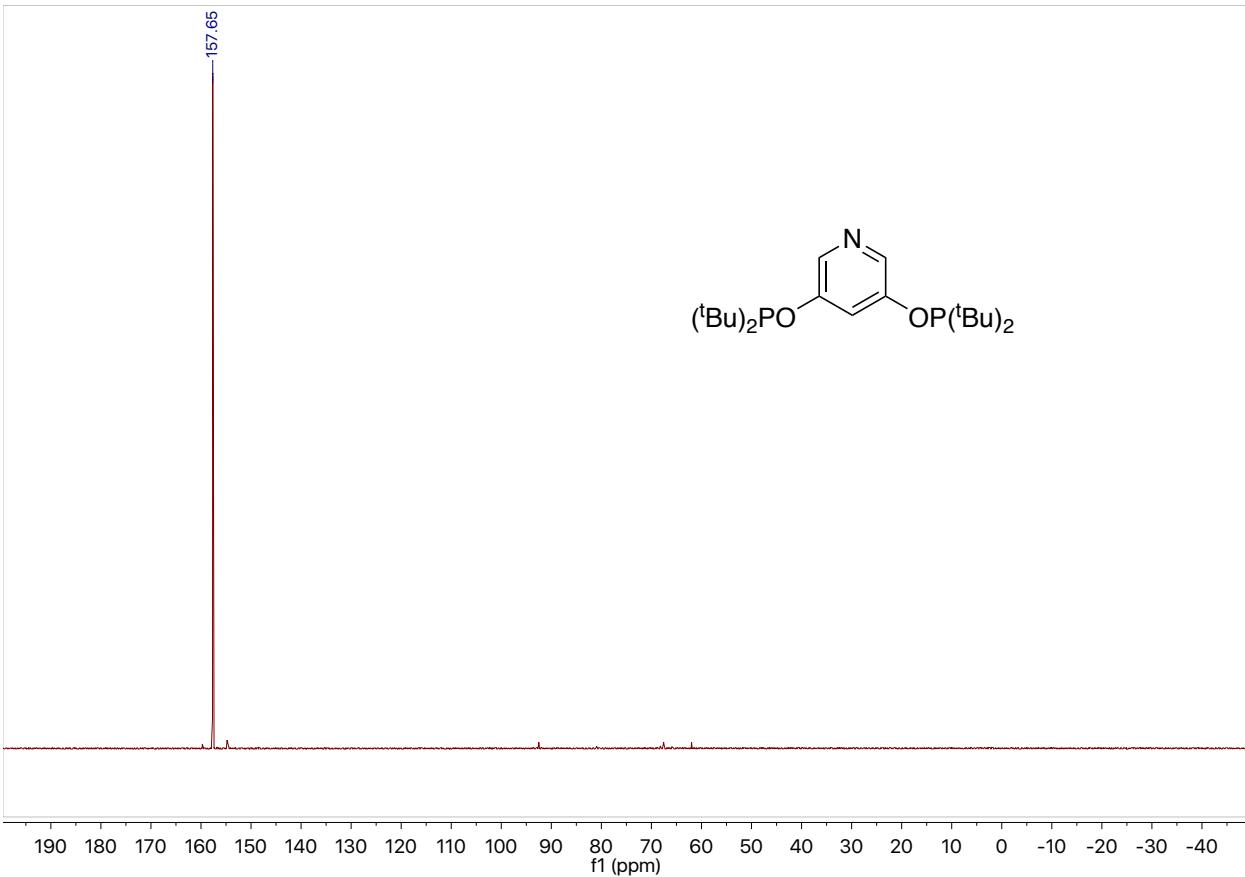
Figure S3. $^{31}P\{^1H\}$ NMR (162 MHz, C$_6$D$_6$) spectrum of 3,5-bis(di-*tert*-butylphosphinito)pyridine, **1**.
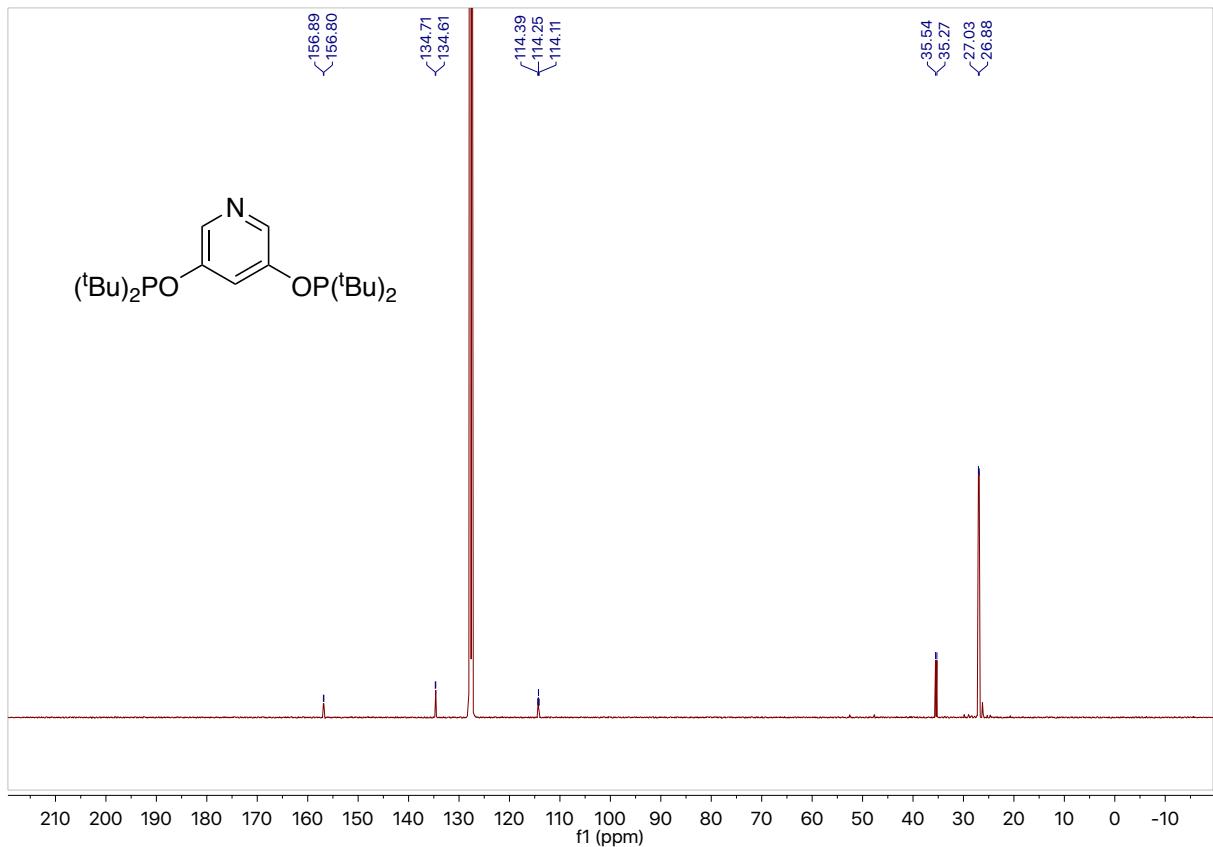
**Figure S4.** $^{13}C\{^1H\}$ NMR (101 MHz, C$_6$D$_6$) of 3,5-bis(di-*tert*-butylphosphinito)pyridine, **1**.
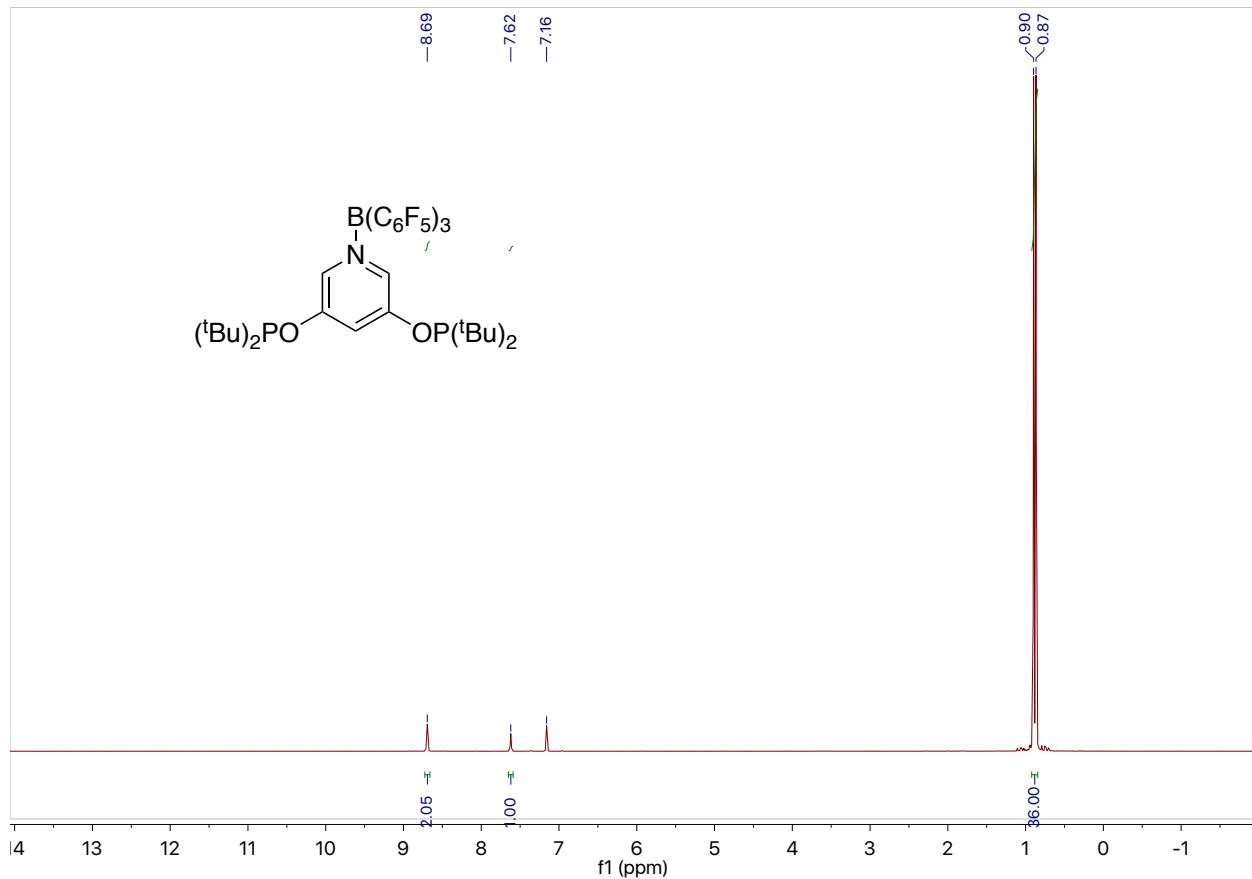
Figure S5. ^{1}H NMR (400 MHz, C$_6$D$_6$) spectrum of *N*-tris(pentafluorophenyl)borane-3,5-bis(di-*tert*-butylphosphinito)pyridine, **2**.
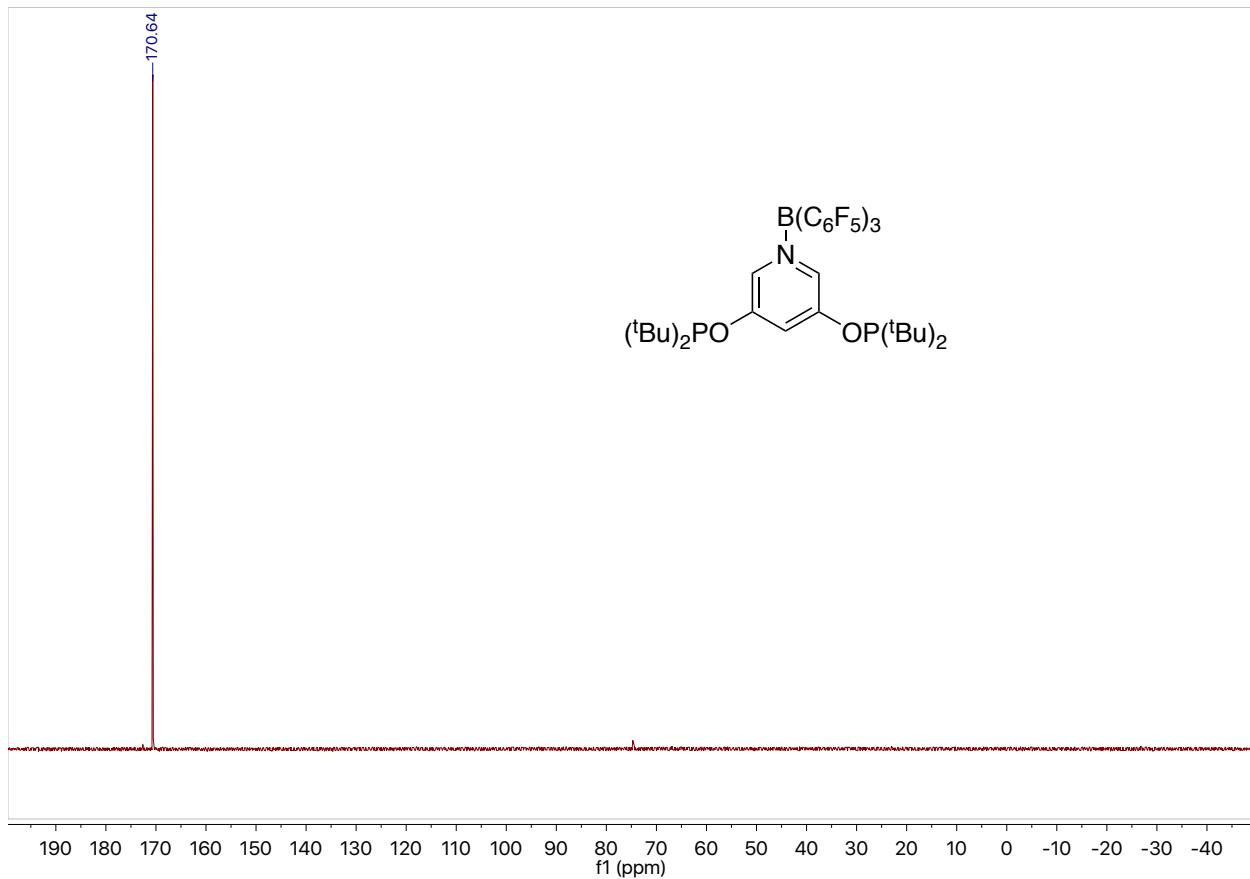
Figure S6. $^{31}P\{^1H\}$ NMR (162 MHz, C_6D_6) spectrum of *N*-tris(pentafluorophenyl)borane-3,5-bis(di-*tert*-butylphosphinito)pyridine, **2**.
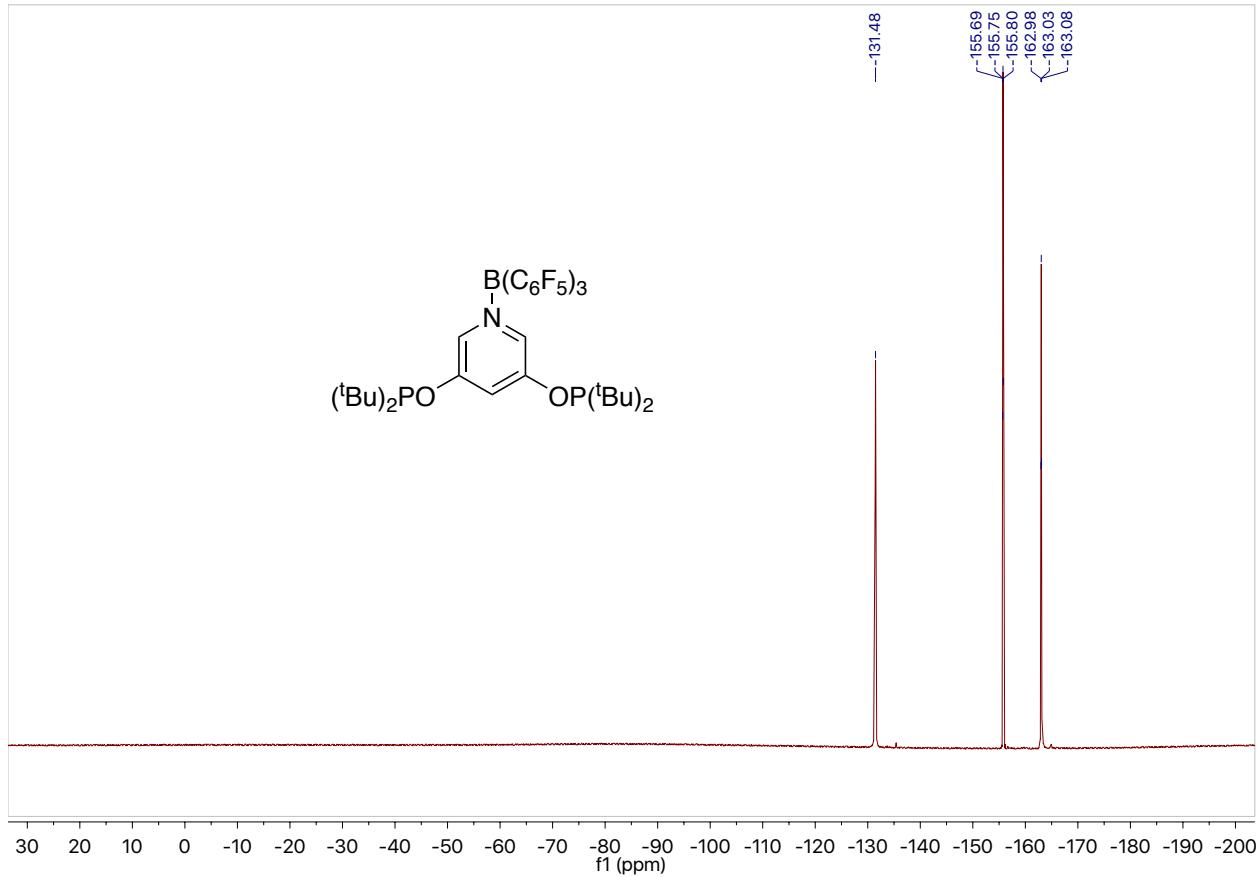
Figure S7. $^{19}F\{^1H\}$ NMR (376 MHz, C$_6$D$_6$) spectrum of *N*-tris(pentafluorophenyl)borane-3,5-bis(di-*tert*-butylphosphinito)pyridine, **2**.
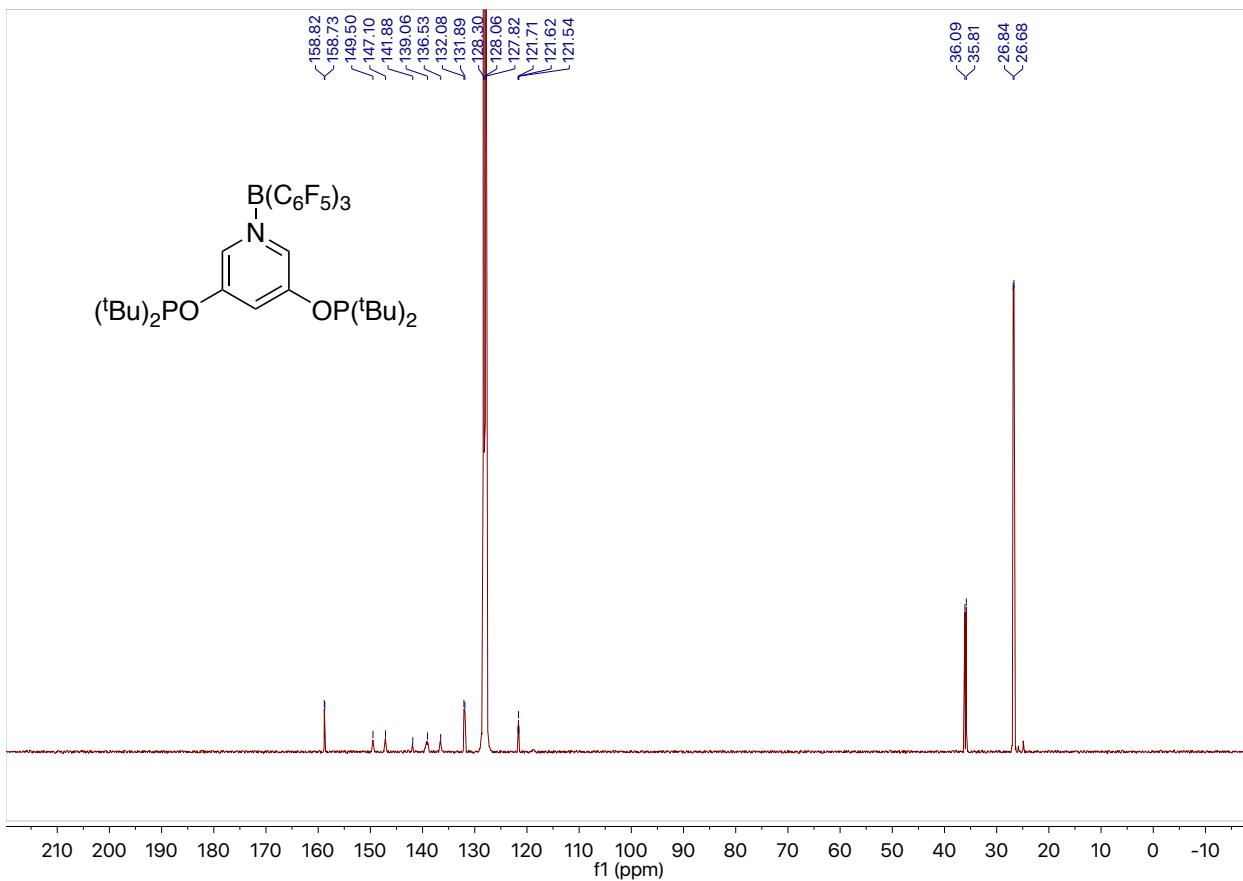
**Figure S8.** $^{13}C\{^1H\}$ NMR (101 MHz, C_6D_6) of *N*-tris(pentafluorophenyl)borane-3,5-bis(di-*tert*-butylphosphinito)pyridine, **2.**
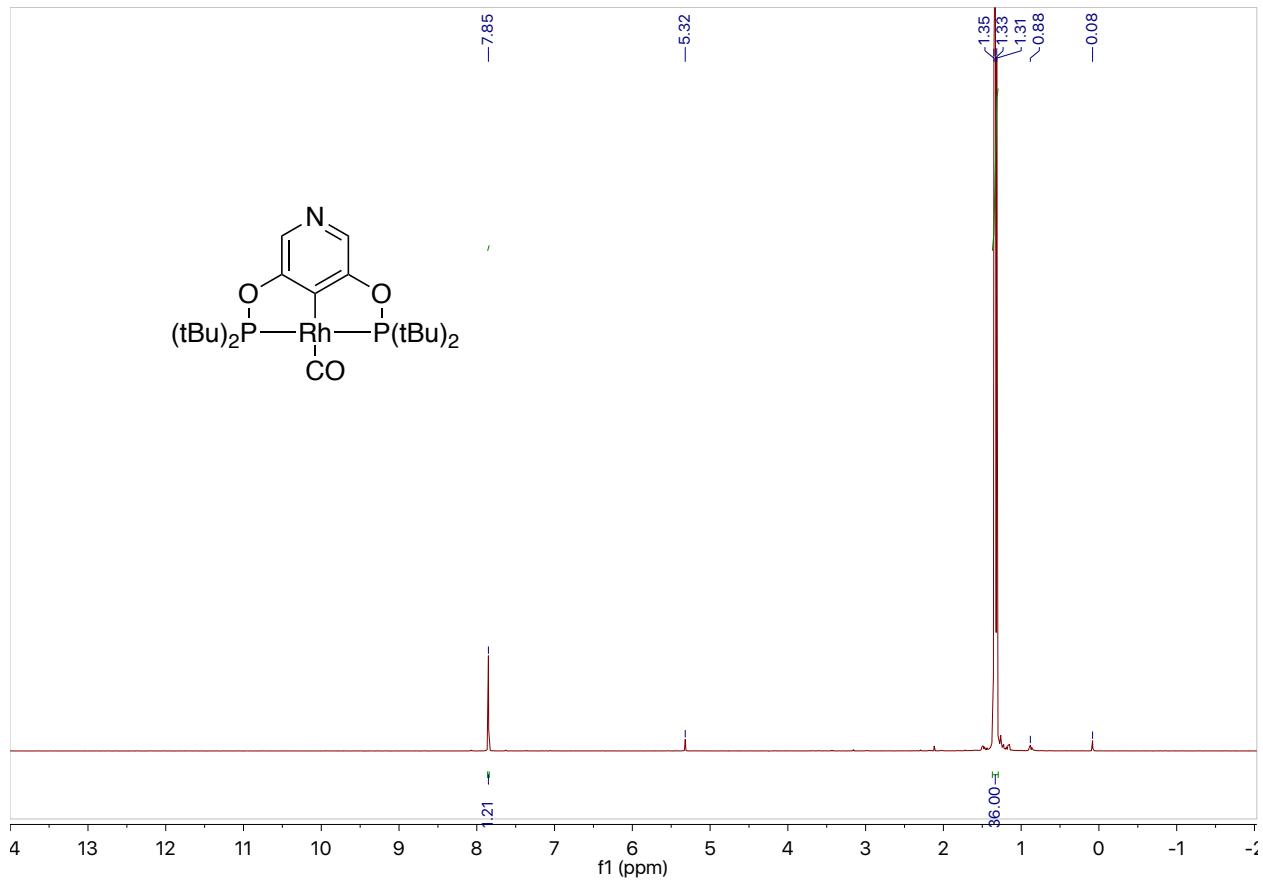
Figure S9. ^{1}H NMR (400 MHz, CD$_2$Cl$_2$) spectrum of (PyPOCOP)Rh(CO), **3**. Contamination by small amounts of silicone grease and pentane is present.
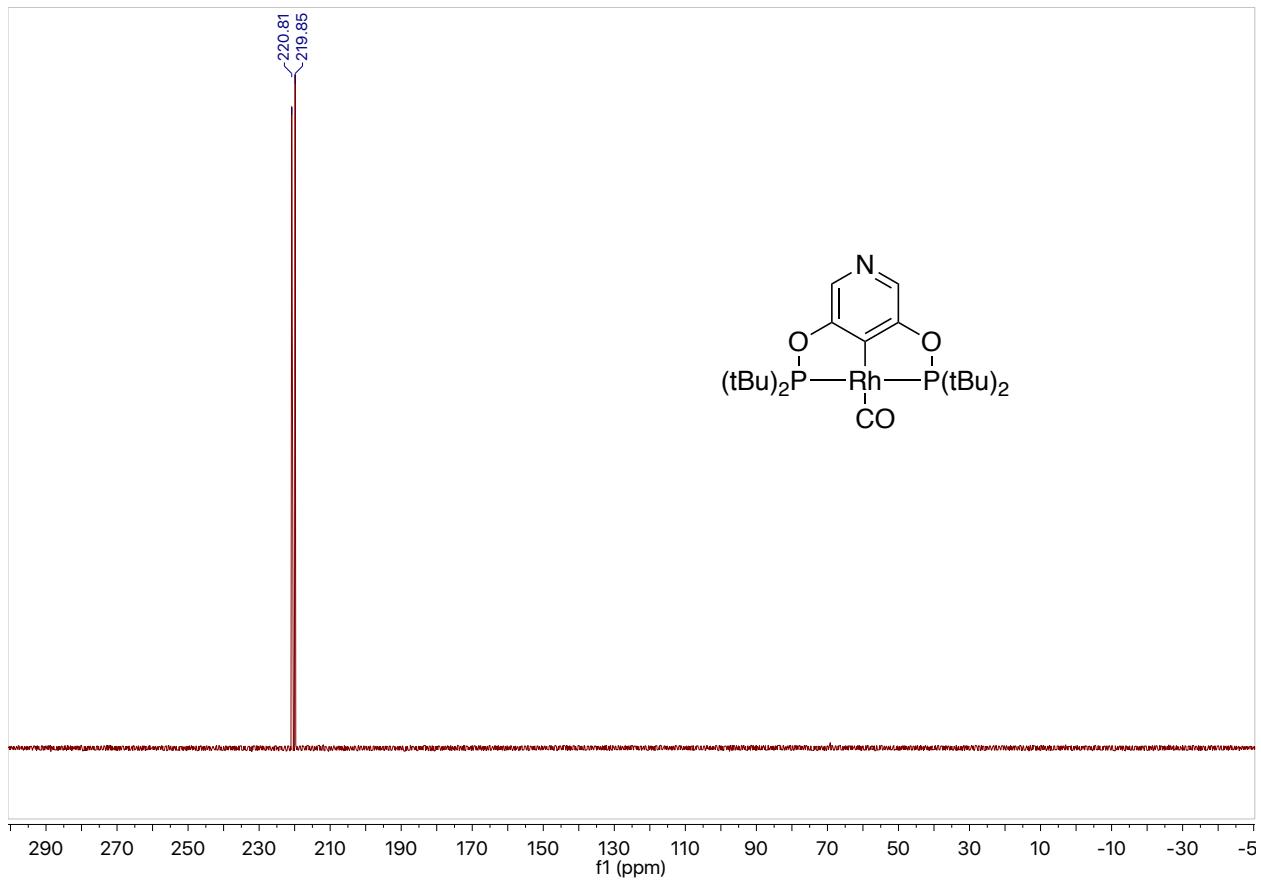
Figure S10. $^{31}P\{^1H\}$ NMR (162 MHz, CD$_2$Cl$_2$) spectrum of (PyPOCOP)Rh(CO), **3**.
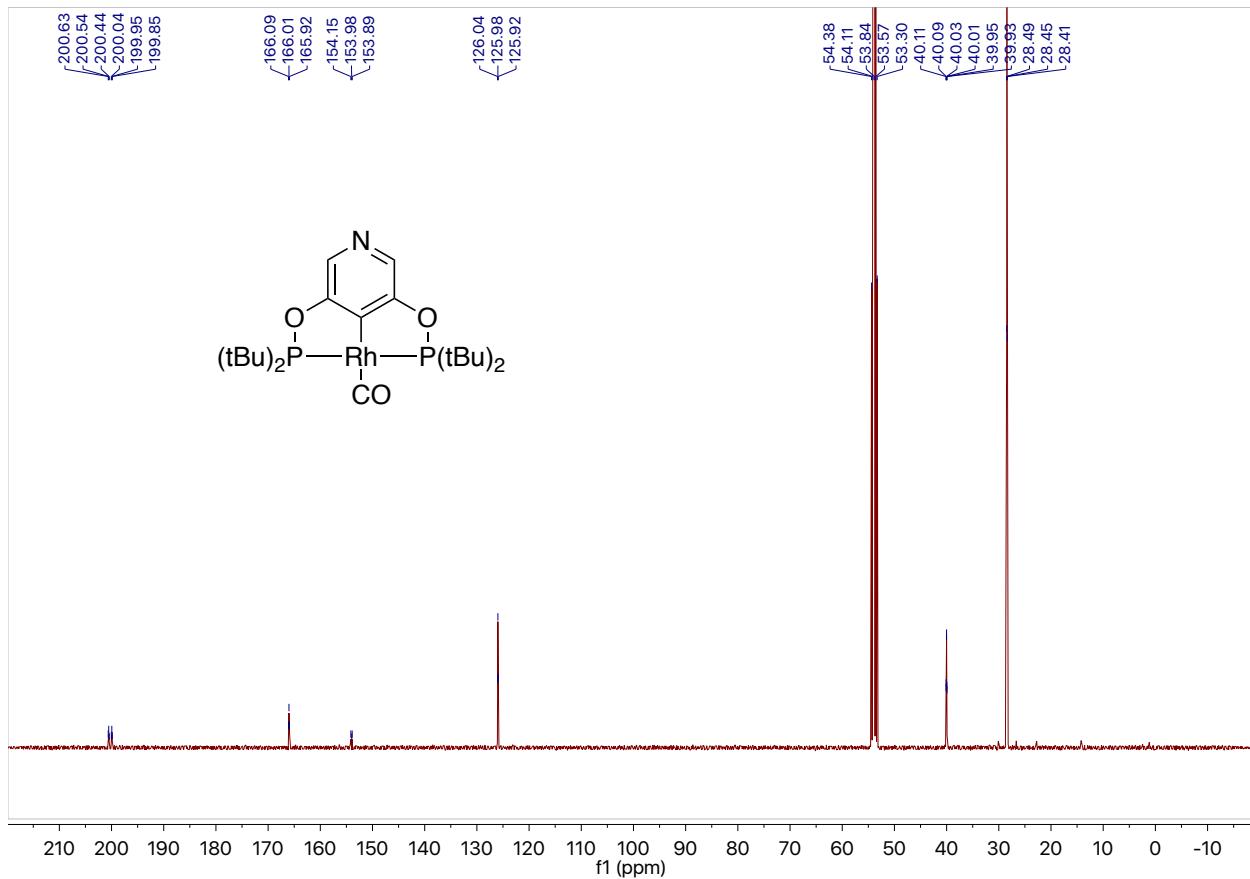
Figure S11. $^{13}C\{^1H\}$ NMR (101 MHz, CD_2Cl_2) of (PyPOCOP)Rh(CO), **3**.
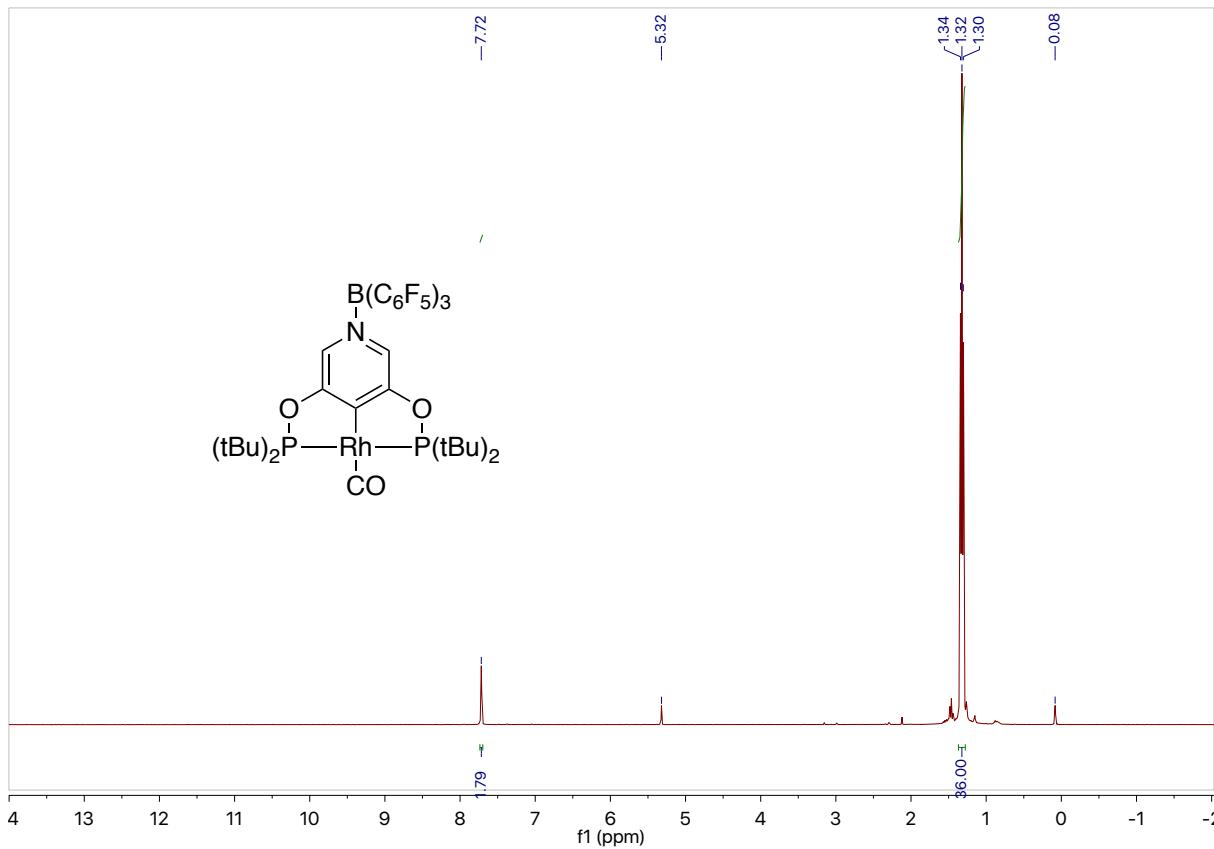
Figure S12. ^{1}H NMR (400 MHz, CD$_2$Cl$_2$) spectrum of (BCF-PyPOCOP)Rh(CO), **4**. Contamination by a small amount of silicone grease is present.
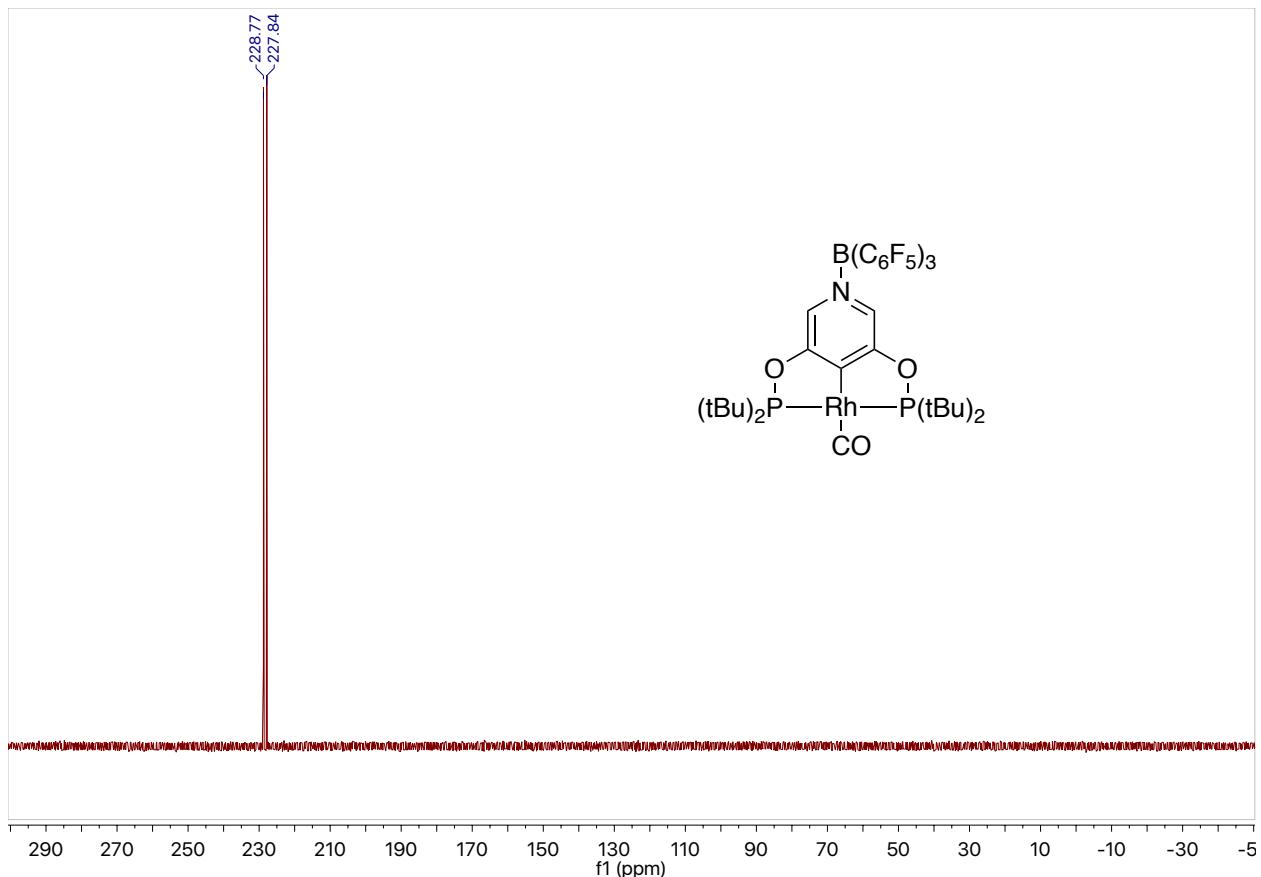
Figure S13. $^{31}P\{^1H\}$ NMR (162 MHz, CD$_2$Cl$_2$) spectrum of (BCF-PyPOCOP)Rh(CO), **4**.
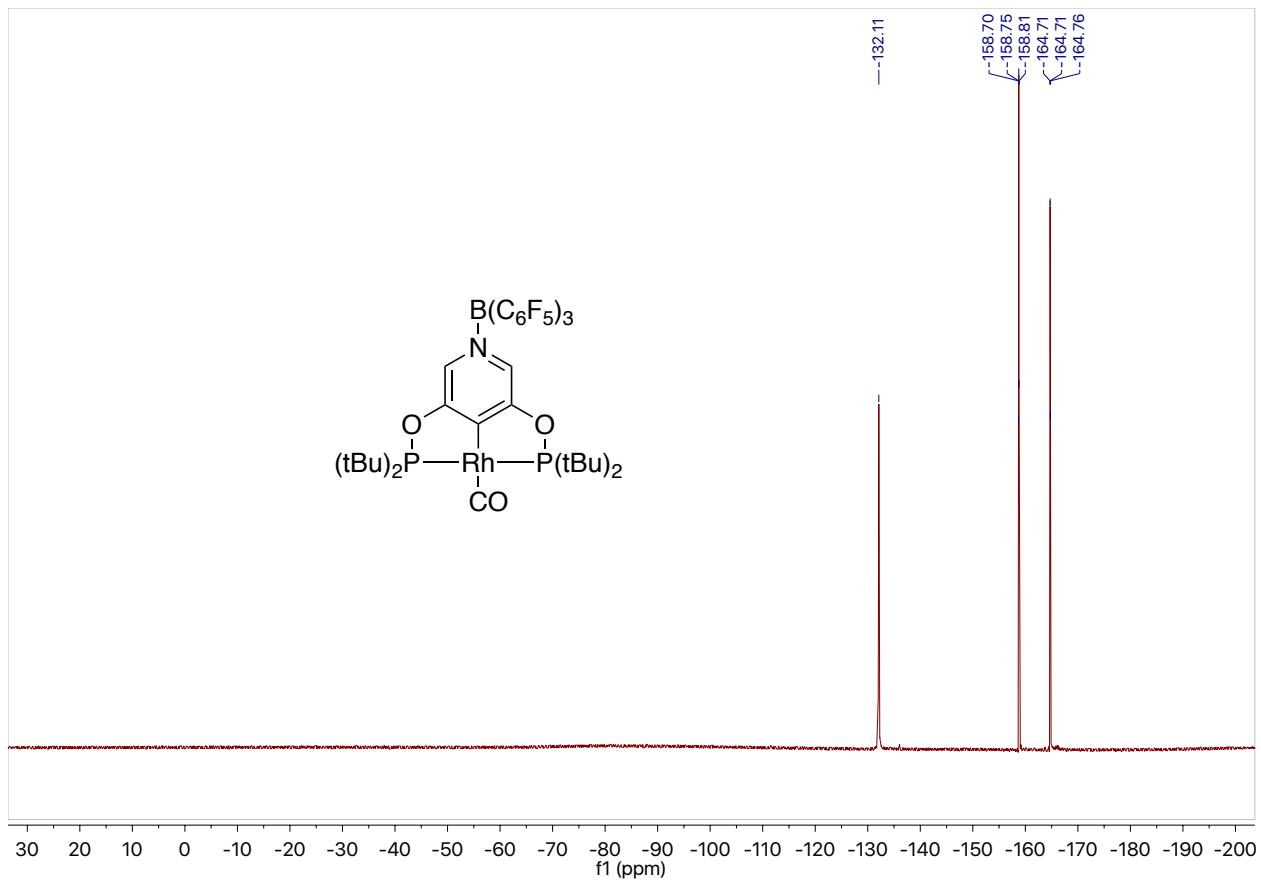
Figure S14. $^{19}F\{^1H\}$ NMR (376 MHz, CD_2Cl_2) spectrum of (BCF-PyPOCOP)Rh(CO), **4**.
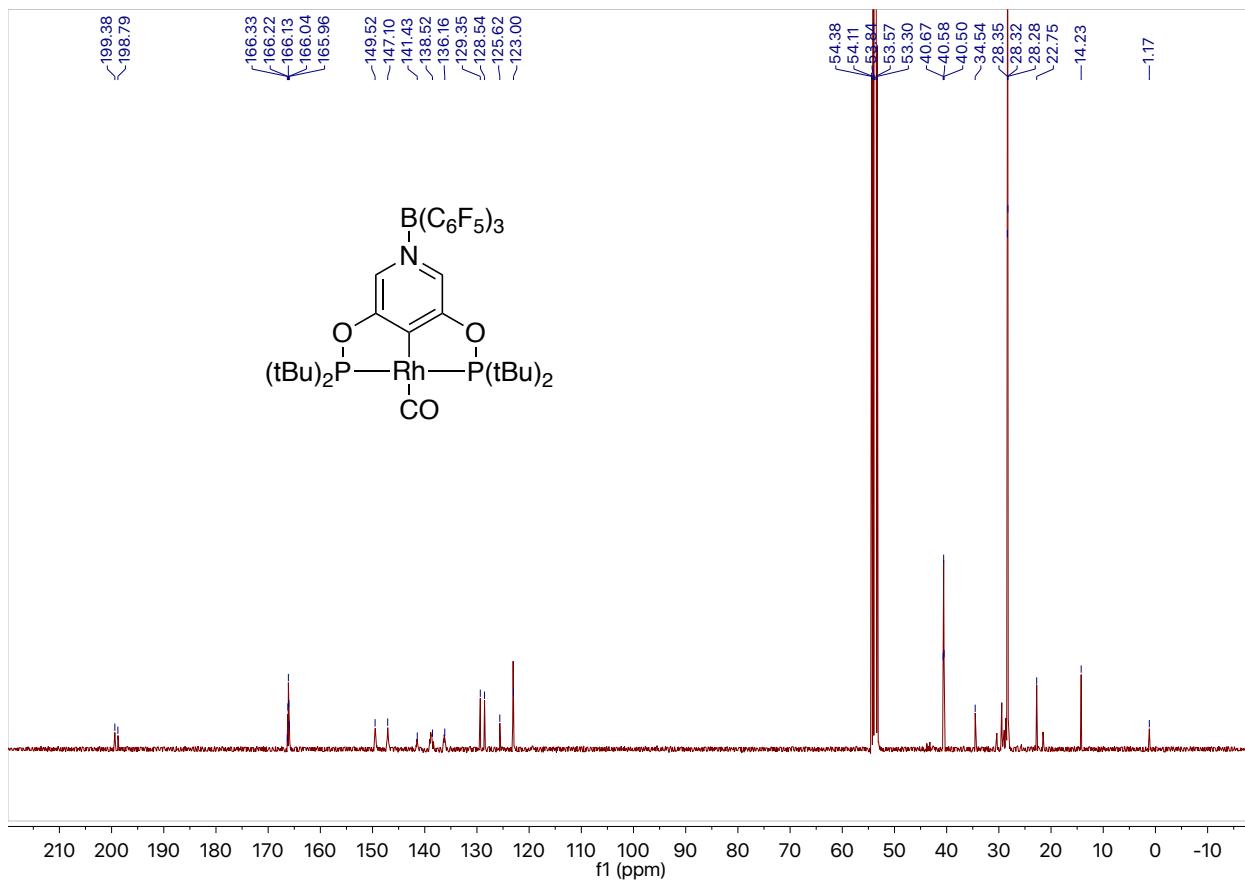
Figure S15. $^{13}C\{^1H\}$ NMR (101 MHz, CD_2Cl_2) of (BCF-PyPOCOP)Rh(CO), **4**.
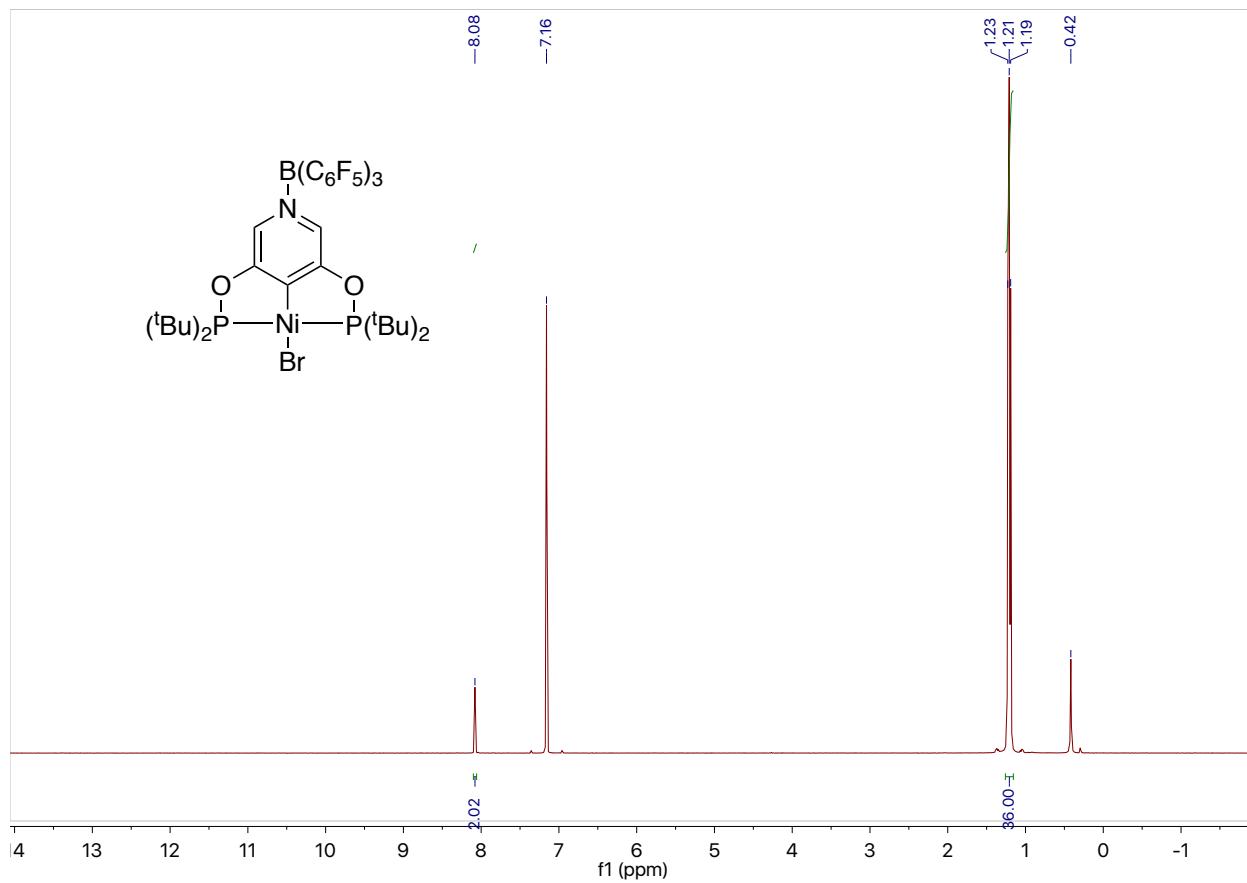
Figure S16. ^{1}H NMR (400 MHz, C_6D_6) spectrum of (BCF-PyPOCOP)NiBr, **5**. Contamination by water is present.
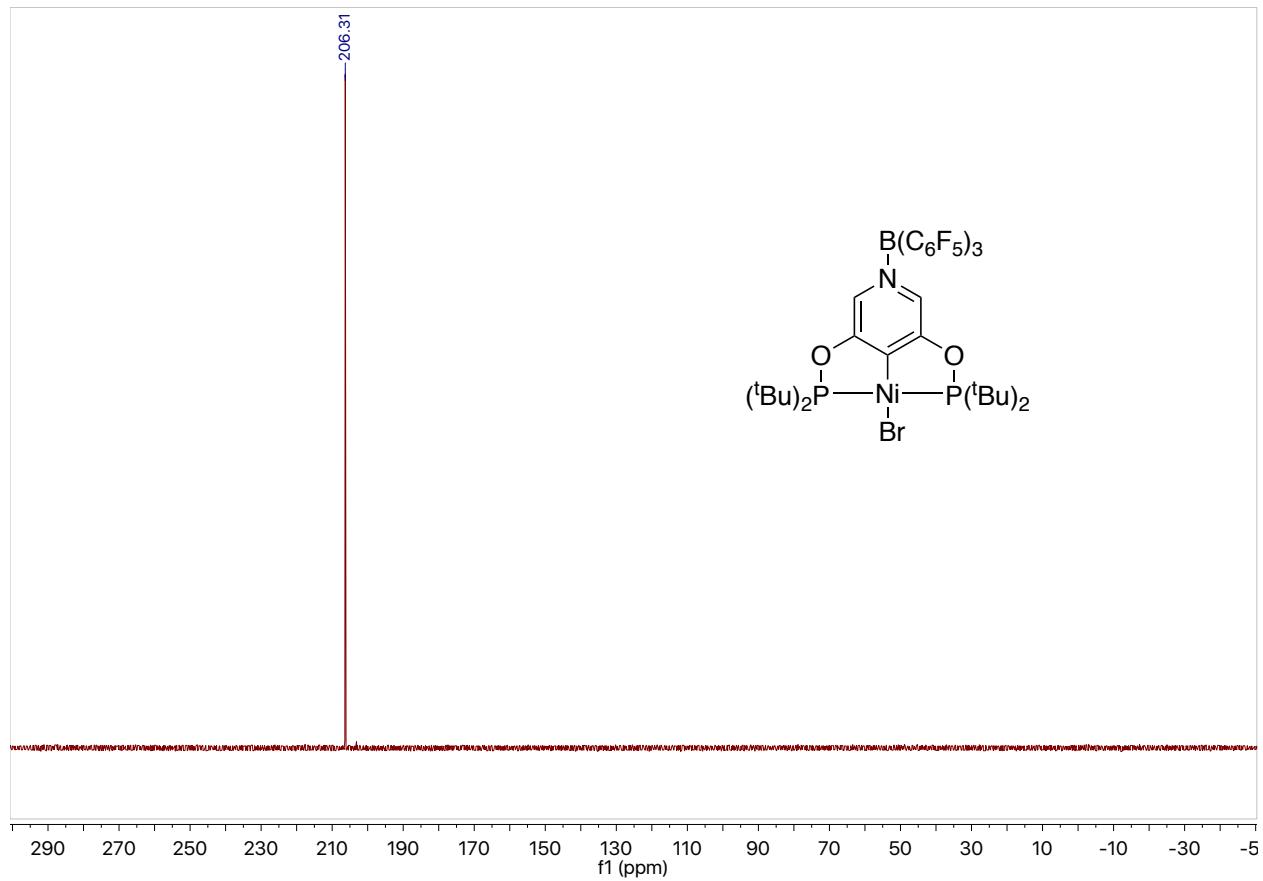
Figure S17. $^{31}P\{^1H\}$ NMR (162 MHz, C$_6$D$_6$) spectrum of (BCF-PyPOCOP)NiBr, **5**.
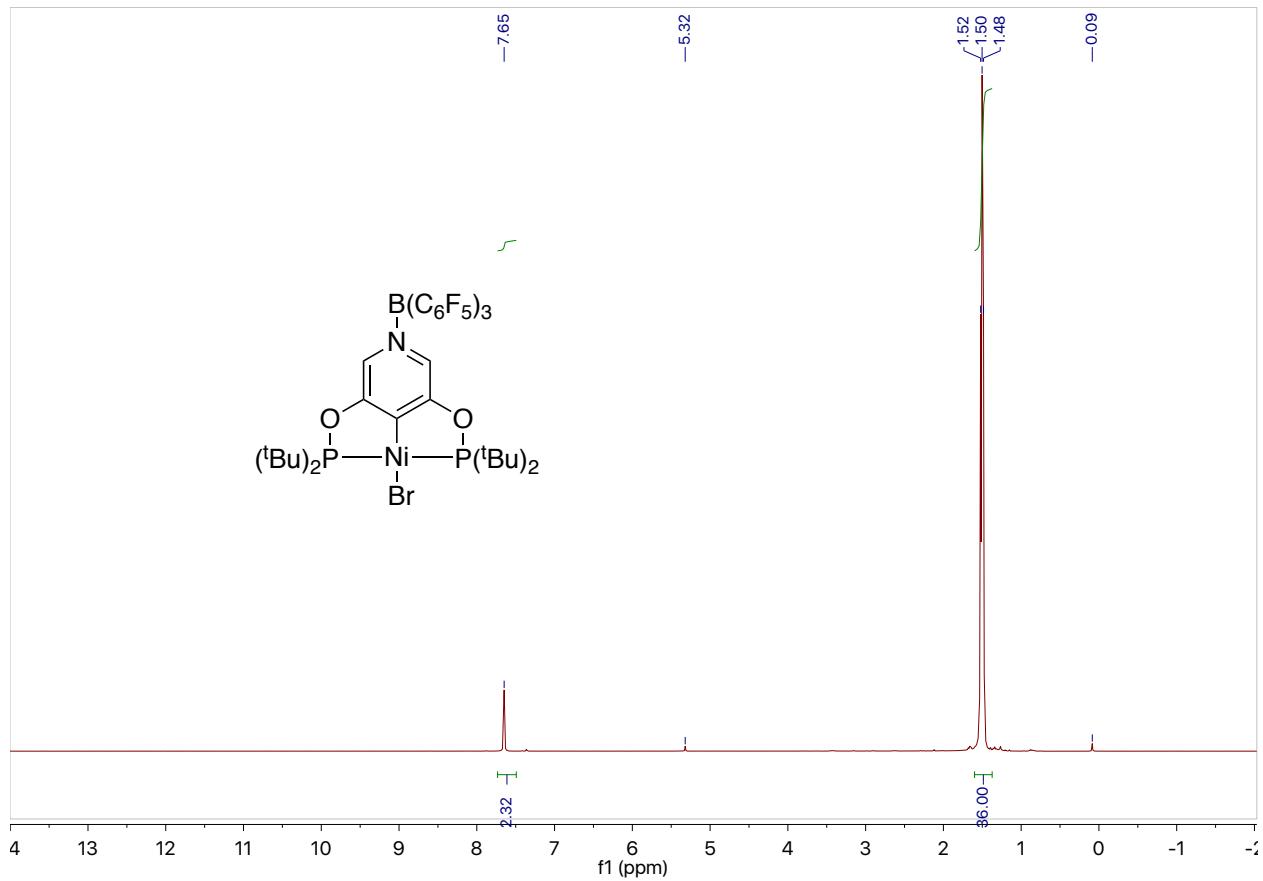
Figure S18. ^{1}H NMR (400 MHz, CD$_2$Cl$_2$) spectrum of (BCF-PyPOCOP)NiBr, **5**. Contamination by a small amount of silicone grease is present.
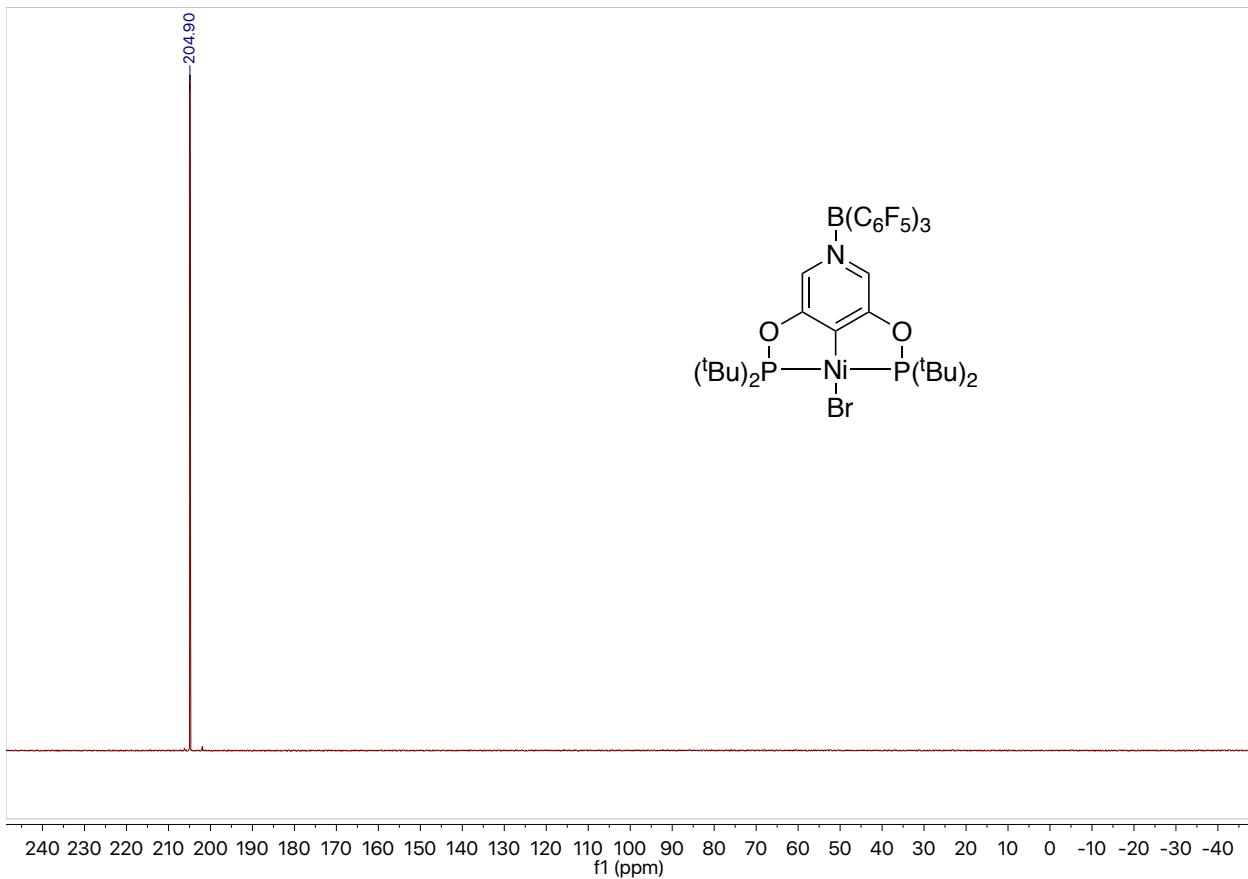
Figure S19. $^{31}P\{^{1}H\}$ NMR (162 MHz, CD$_2$Cl$_2$) spectrum of (BCF-PyPOCOP)NiBr, **5**.
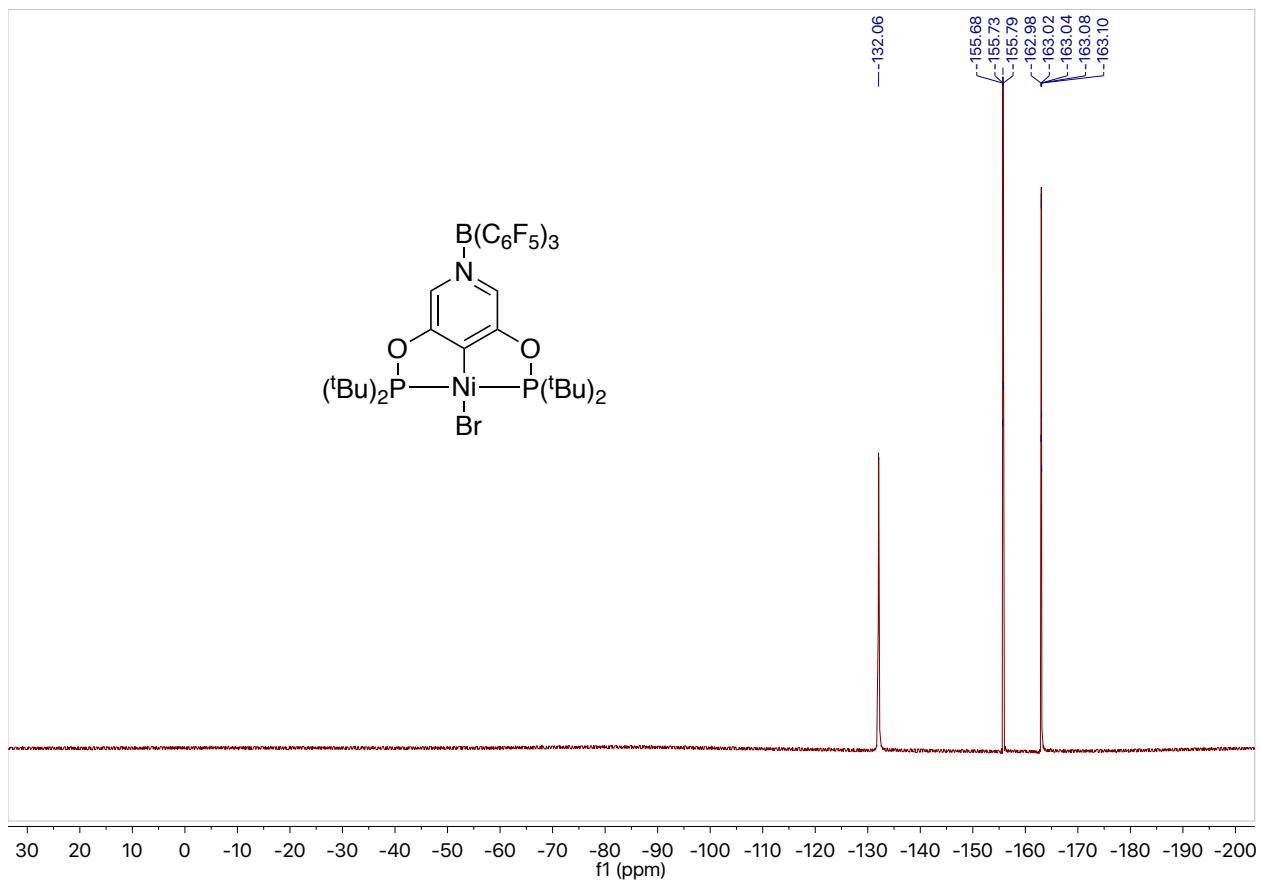
**Figure S20.** $^{19}F\{^1H\}$ NMR (376 MHz, CD_2Cl_2) spectrum of (BCF-PyPOCOP)NiBr, **5**.
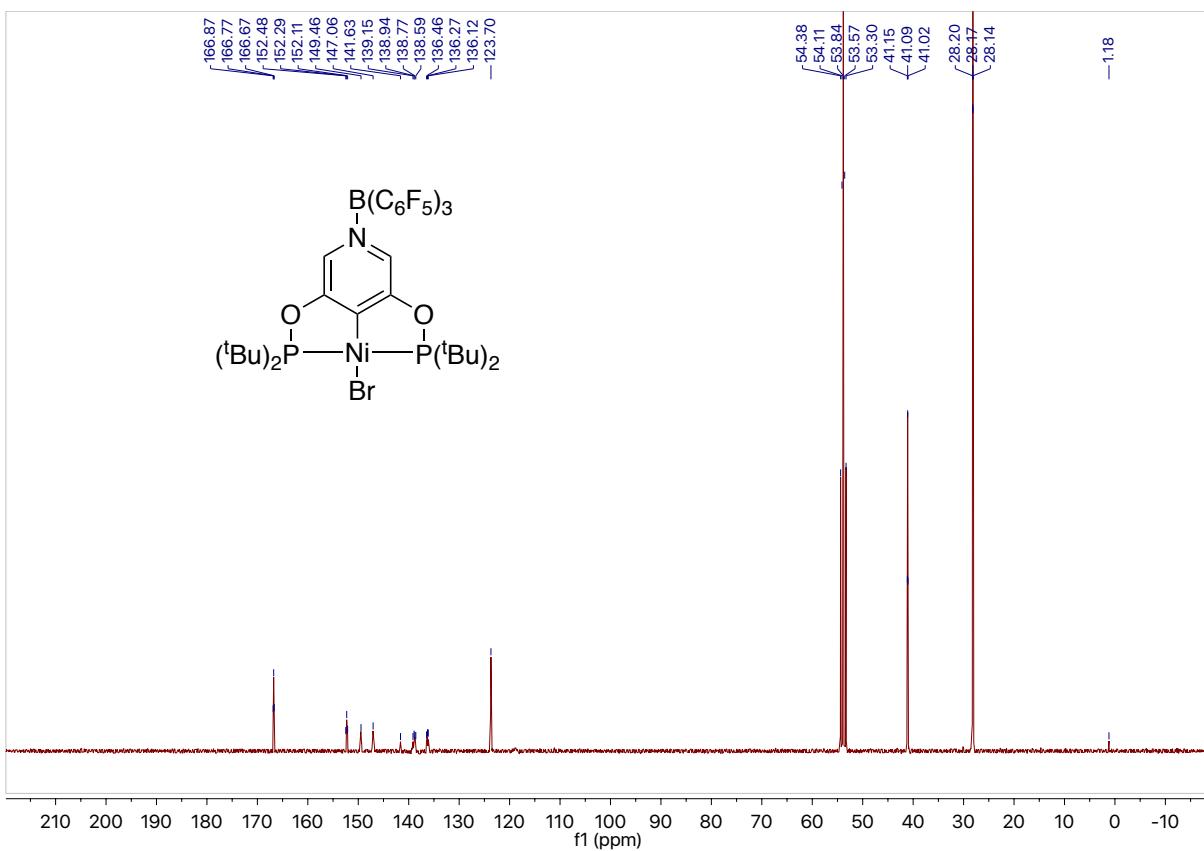
Figure S21. $^{13}C\{^1H\}$ NMR (101 MHz, CD_2Cl_2) of (BCF-PyPOCOP)NiBr, **5**. Contamination by a small amount of silicone grease is present.
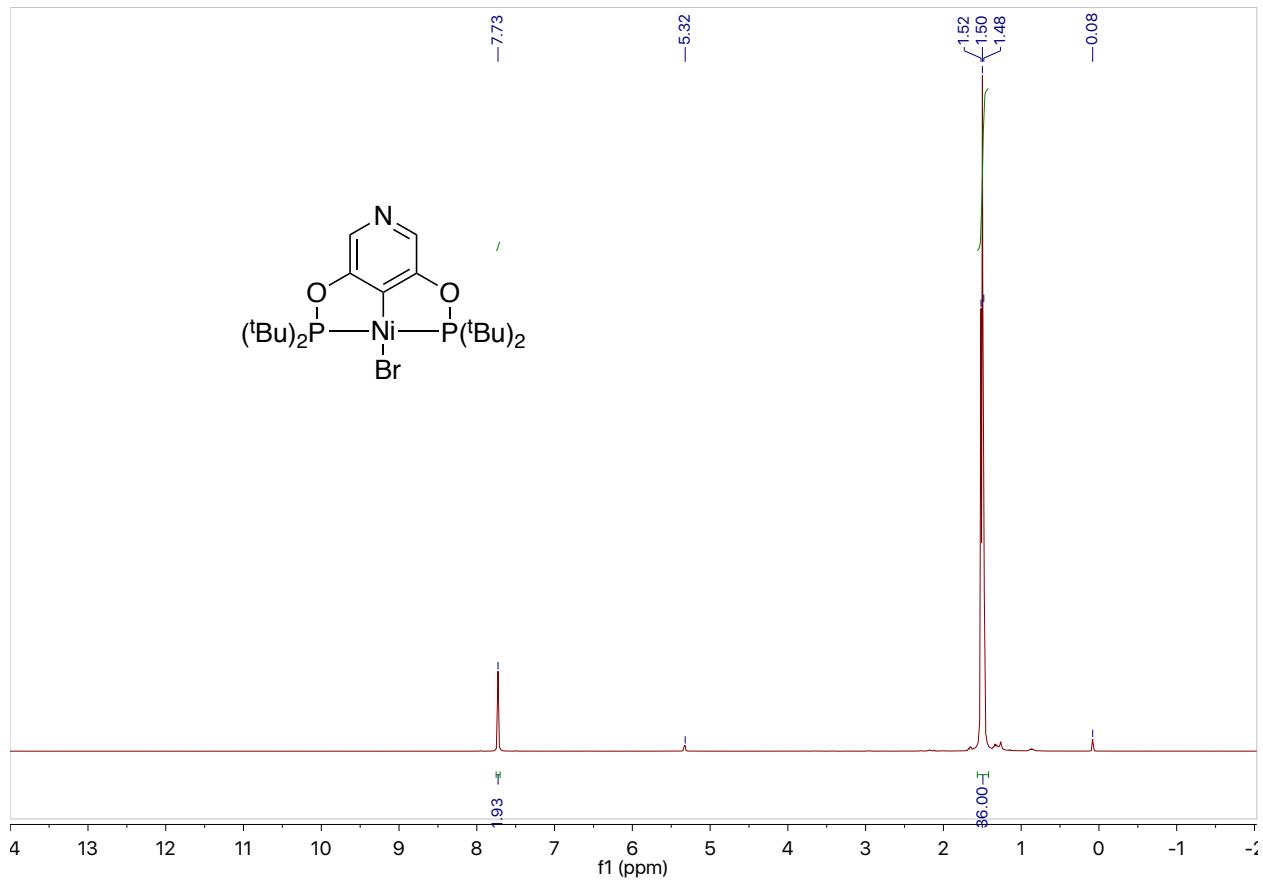
Figure S22. ^{1}H NMR (400 MHz, CD$_2$Cl$_2$) spectrum of (PyPOCOP)NiBr, **6**. Contamination by a small amount of silicone grease is present.
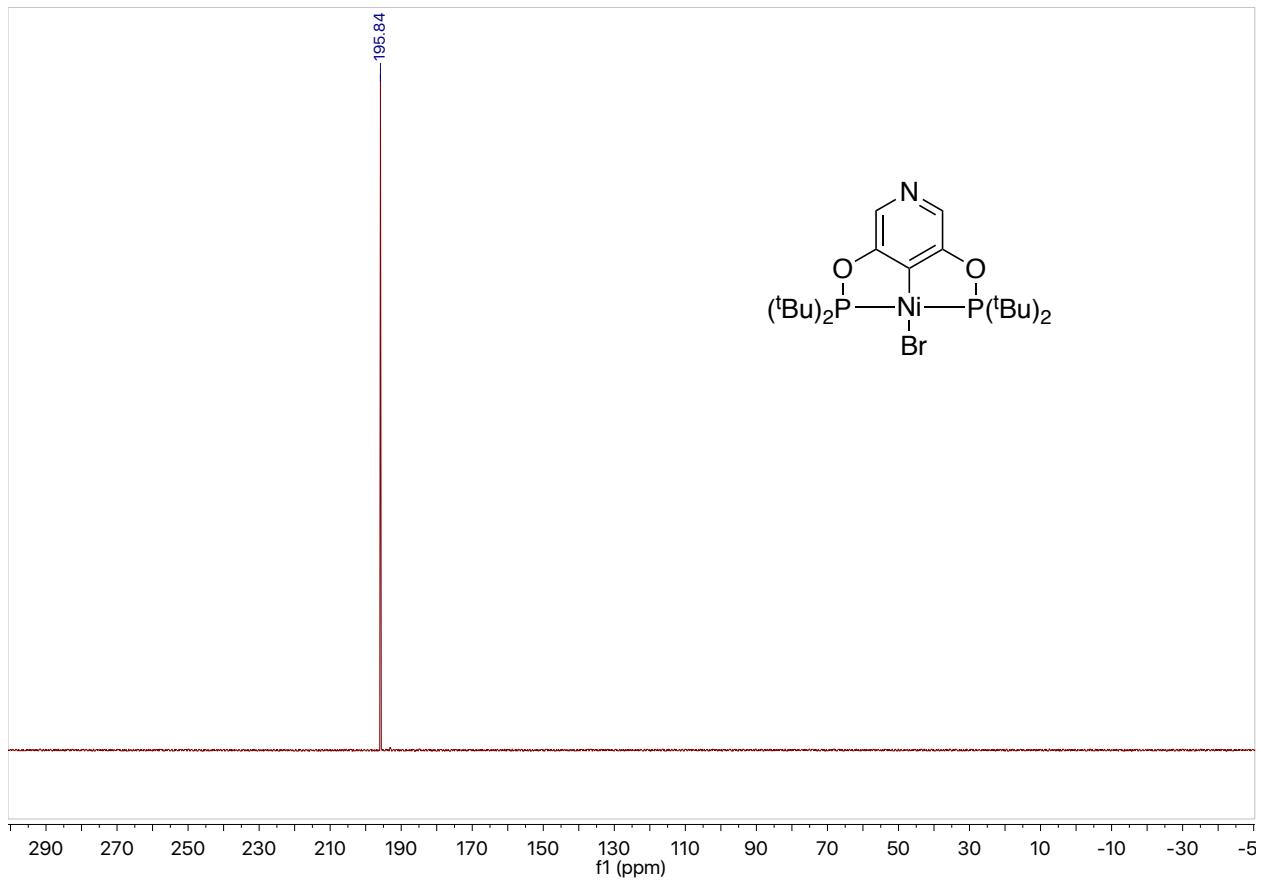
**Figure S23**. $^{31}P\{^1H\}$ NMR (162 MHz, CD$_2$Cl$_2$) spectrum of (PyPOCOP)NiBr, **6**.
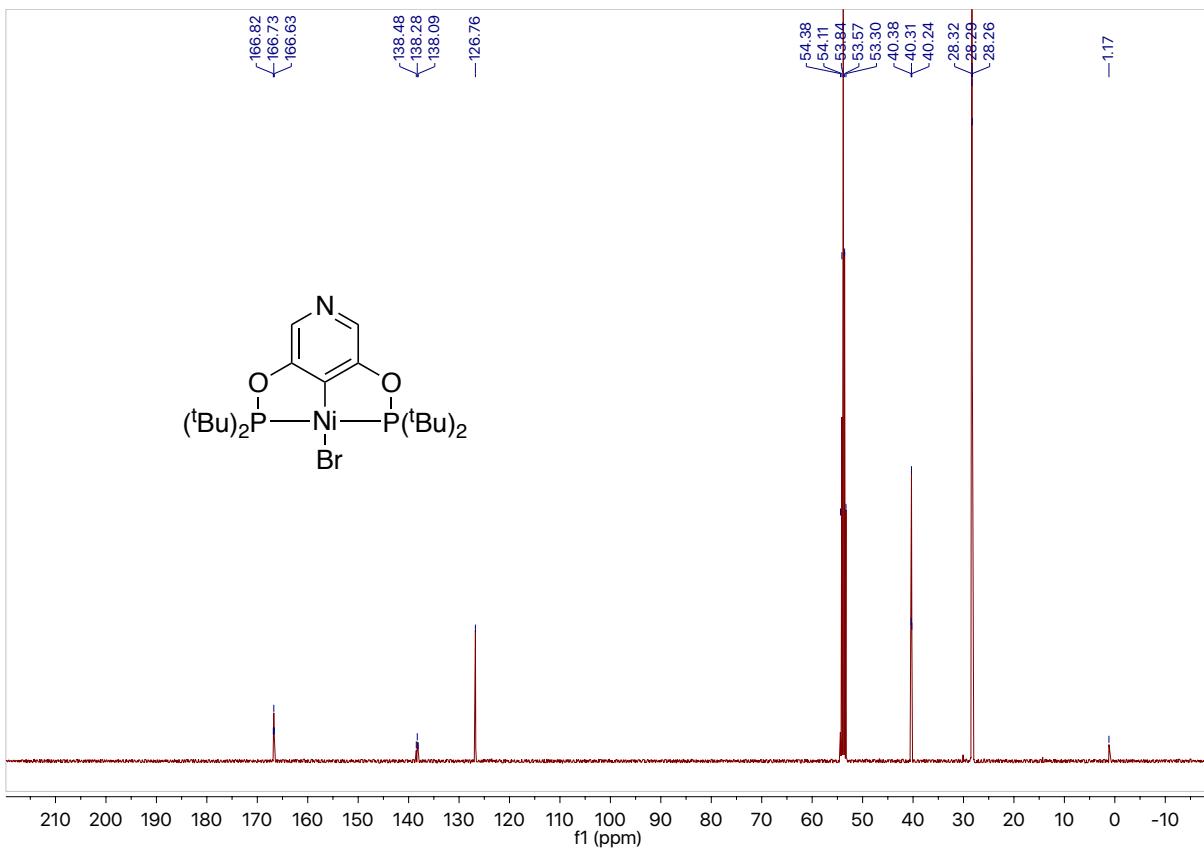
**Figure S24.** $^{13}C\{^1H\}$ NMR (101 MHz, CD_2Cl_2) of (PyPOCOP)NiBr, **6**. Contamination by a small amount of silicone grease is present.

Infrared Spectra
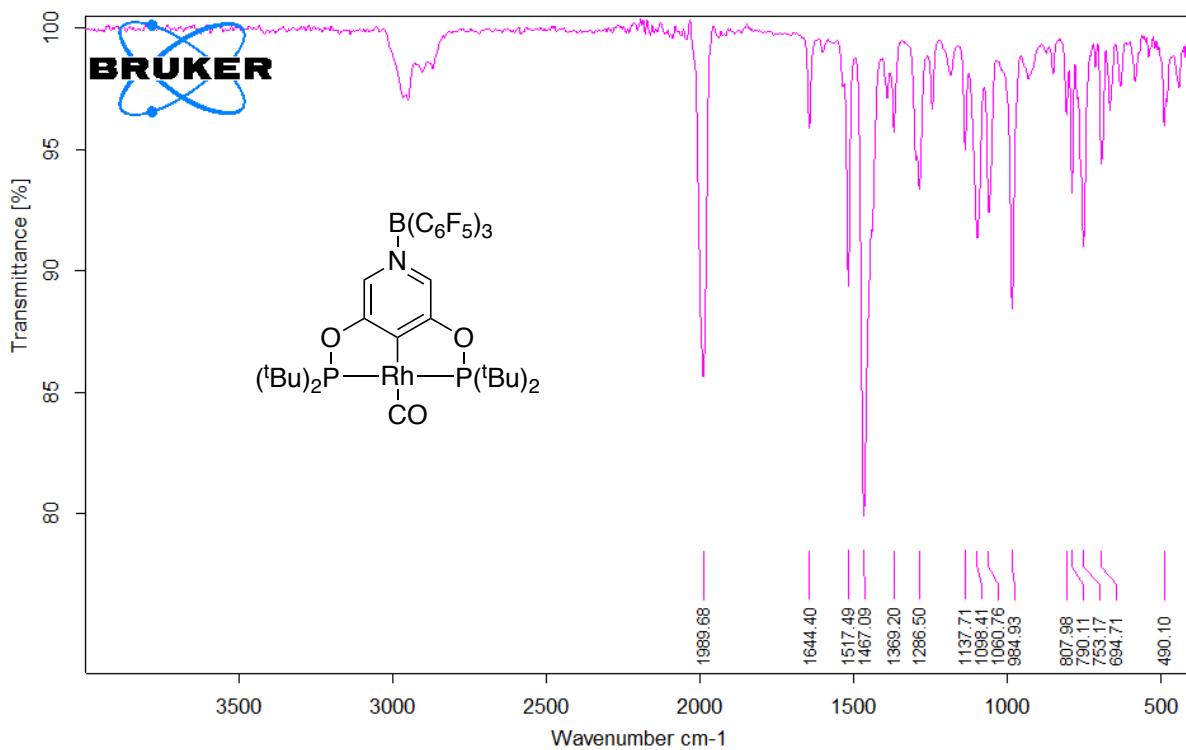
Figure S25. IR spectrum (ATR-IR, thin film THF) of (BCF-PyPOCOP)Rh(CO), **4**.
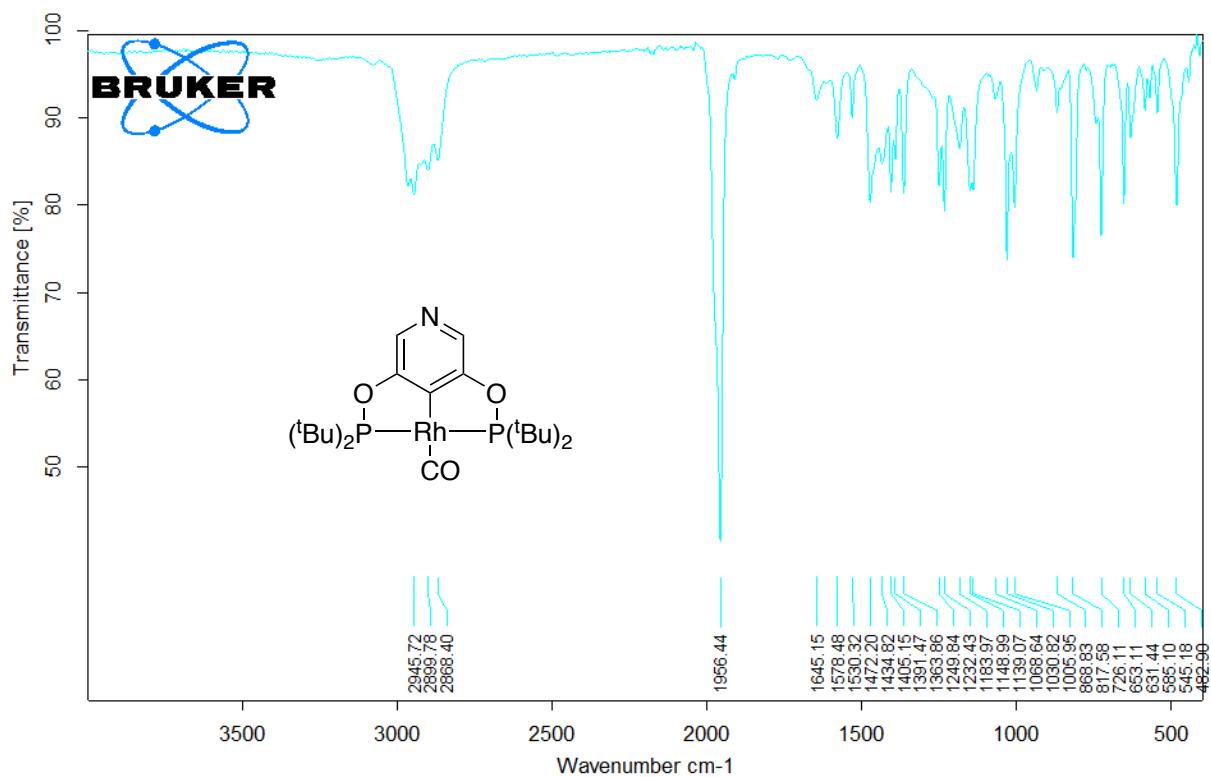
Figure S26. IR spectrum (ATR-IR, thin film THF) of (PyPOCOP)Rh(CO), **3.**

Cyclic Voltammetry
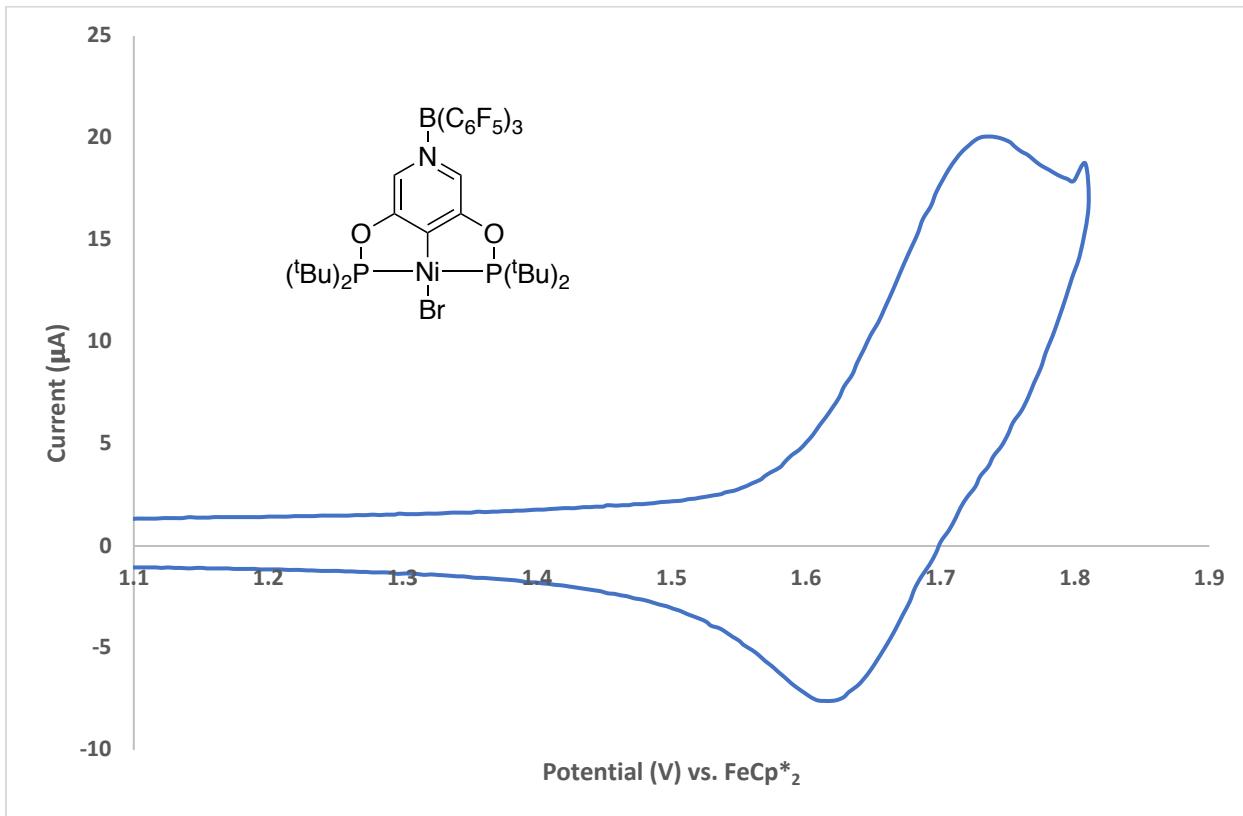
Figure S27. Cyclic voltammogram of complex **5** in CH$_2$Cl$_2$ with 0.1 M (*n*-Bu$_4$N)(PF$_6$) electrolyte. $E_{1/2}$ = 1.68 V and E_{ox} = 1.74 V vs. decamethylferrocene.
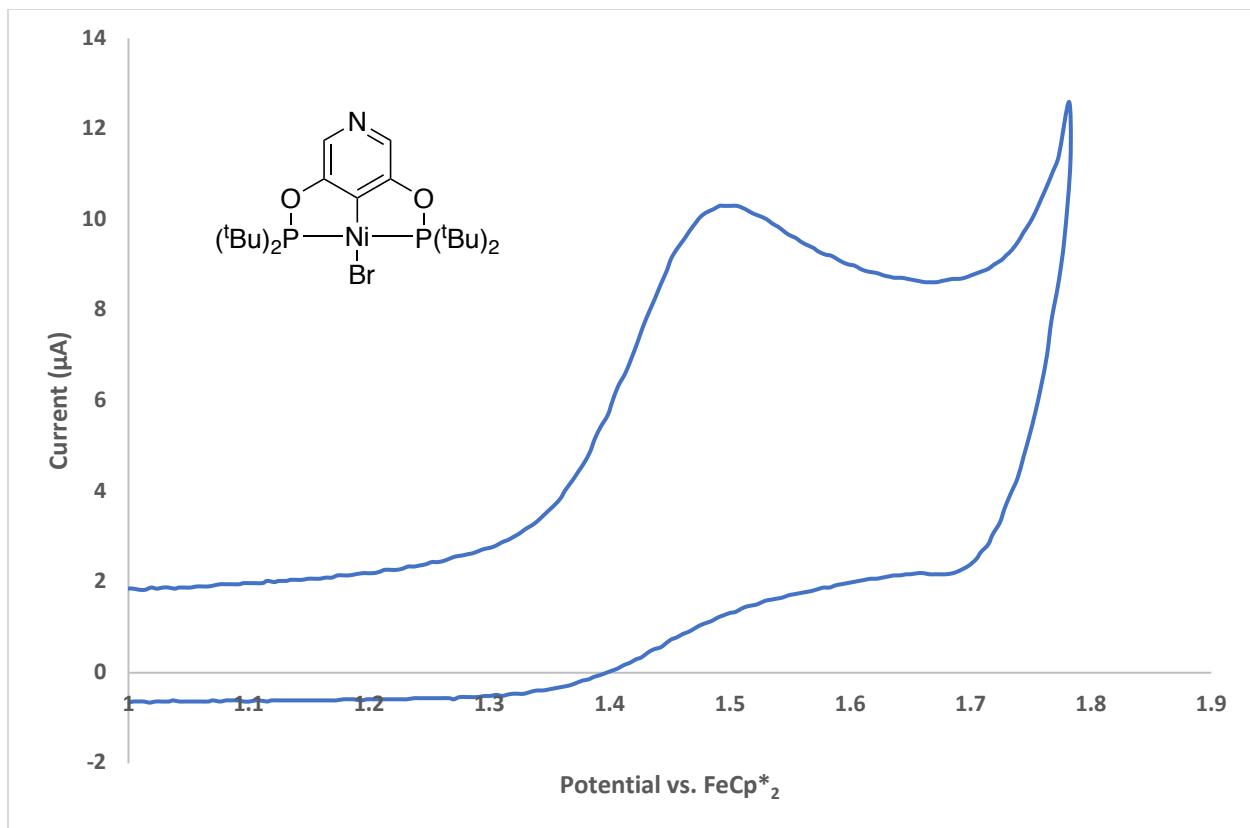
Figure S28. Cyclic voltammogram of complex **6** in CH_2Cl_2 with 0.1 M (n-Bu$_4$N)(PF$_6$) electrolyte. E_{ox} = 1.749V vs. decamethylferrocene.

X-Ray Structure Determination

Compound 5 (BCF-PyPOCOP)NiBr

Low-temperature diffraction data (ϕ-and ω-scans) were collected on a Bruker AXS D8 VENTURE KAPPA diffractometer coupled to a PHOTON 100 CMOS detector with Mo K_α radiation ($\lambda = 0.71073$ Å) from an IμS micro-source for the structure of compound **5**. The structure was solved by direct methods using SHELXS and refined against F^2 on all data by full-matrix least squares with SHELXL-2016 using established refinement techniques.[1-3] All non-hydrogen atoms were refined anisotropically. All hydrogen atoms were included into the model at geometrically calculated positions and refined using a riding model. The isotropic displacement parameters of all hydrogen atoms were fixed to 1.2 times the U value of the atoms they are linked to (1.5 times for methyl groups).

Compound **5** crystallizes in the monoclinic space group $P2_1/n$ with one molecule in the asymmetric unit.

Empirical formula	C39 H38 B Br F15 N Ni O2 P2
Formula weight	1049.07
Temperature	100(2) K
Wavelength	0.71073 Å
Crystal system	Monoclinic
Space group	$P2_1/n$
Unit cell dimensions	a=18.331(2) Å
	α= 90°.
b = 12.0823(15) Å	β= 99.077(5)°.
c = 19.875(3) Å	γ = 90°.
Volume	4346.9(9) Å^3
Z	4
Density (calculated)	1.603 Mg/m^3
Absorption coefficient	1.539 mm-1
F(000)	2112
Crystal size	0.450 x 0.450 x 0.400 mm^3
Theta range for data collection	2.250 to 36.417°.
Index ranges	-28<=h<=30, -20<=k<=20, -33<=l<=33
Reflections collected	151341
Independent reflections	21162 [R(int) = 0.0554]
Completeness to theta = 25.242°	99.9 %
Absorption correction	Semi-empirical from equivalents
Max. and min. transmission	0.7471 and 0.6178
Refinement method	Full-matrix least-squares on F2
Data / restraints / parameters	21162 / 0 / 571
Goodness-of-fit on F2	1.025
Final R indices [I>2sigma(I)]	R1 = 0.0357, wR2 = 0.0693
R indices (all data)	R1 = 0.0611, wR2 = 0.0765
Extinction coefficient	n/a
Largest diff. peak and hole	0.918 and -0.964 e.Å^{-3}

Table S1. Crystal data and structure refinement for complex **5**.

References

1.   Sheldrick, G.M. Phase Annealing in SHELX-90: Direct Methods for Larger Structures. *Acta. Cryst.* **1990**, *A46*, 467-473.

2.   Sheldrick, G.M. A Short History of SHELX. *Acta. Cryst.* **2008**, *A64*, 112-122.

3.   Müller, P. Practical Suggestions for Better Crystal Structures. *Crystallography Reviews* **2009**, *15*, 57-83.